URSI GASS 2021, Rome, Italy, 28 August - 4 September 2021

Dual-Polarized Holographic Transmitarray for Flat-top Beams Synthesis

Lamine N.A Bamogho, Jean-Jacques Laurin
Department of Electrical Engineering, Poly-Grames Research Center
Polytechnique Montréal, Montréal, Canada
lamine-asmarane.bamogho@polymtl.ca;jean-jacques.laurin@polymtl.ca

Abstract

A synthesis method to realize dual orthogonally-polarized coverage based on Holographic Transmitarray (HTA) is presented. The HTA consists of a Transmitarray Antenna in which the unit cell phases are obtained with a modified version of the Gerchberg-Saxton algorithm (TA-GS) The performance of the proposed method is demonstrated by the synthesis of a flat-top concentric coverages (DP-DFC). Dual polarization is generated from an anisotropic transmitarray unit-cell, which is based on four stacked layers achieving independent 360-degree phase ranges for both linear polarizations. The numerical results verify the rapid convergence of proposed TA-GS method and demonstrate its ability to synthetize a flat-top far-field pattern. The demonstrated DP-DFC capabilities make them a potential candidate for implementations in satellite communications.

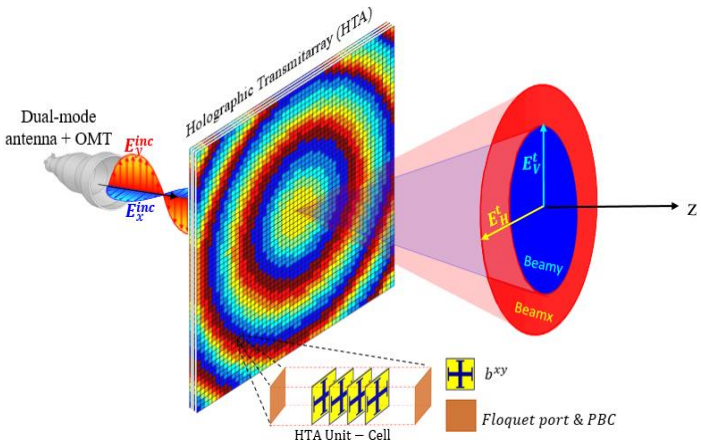

Figure 1: 3D scheme of Dual-polarized flat-top concentric coverages antenna.

1 Introduction

The ever-growing market demand for high throughput satellites has triggered the present research towards the development of novel wireless systems with improved performance. An approach to enhance throughput is to communicate through multiple channels and multi-modes in parallel. However, this results in higher interference between the corresponding communication channels and isolating them is challenging. In general, frequency and/or polarization diversity are exploited to achieve this isolation. Moreover, high-gain antennas with pencil beam radiation patterns can also be utilized to achieve an additional isolation in space between the communication channels.

To date, high-gain antennas such as 3D lenses, reflectors, and phased-arrays have been the primary choice and dominated a wide range of applications [1]. However, planar transmitarray antennas (TAs) are emerging to replace the traditional high-gain antennas in numerous deployments, as they are easy-to-fabricate, light-weight, and inexpensive. In addition, unlike the reflectarray antennas (RAs), TAs do not suffer from feed blockage, which leads to higher aperture efficiency. A study on dual-polarized TAs for frequency-reuse communication systems has been reported in [2], where the spectrum capacity has been enhanced through two transmission channels. Moreover, TAs are also appropriate for implementation in the beam collimation applications with fixed beam or beam scanning purposes as reported in [3] and [4]. In addition, they are also able to synthetize power radiation patterns to satisfy the flat-top radiation pattern for satellite multibeam missions [5]. In spite of these notable advantages and applications of the dual-polarized TAs, limited research has been carried out in synthesizing and realizing them [5], in contrast to the dual-polarization RAs that are investigated by various groups as in [6].

A wide range of evolutionary algorithms are already available in the literature to assist the design of flat-top radiation patterns. Among them, particle swarm optimization (PSO)and genetic algorithms (GA) have demonstrated immense capabilities in single-beam and multi-beam optimization problems[7]. However, they suffer from high side-lobes and ripples in the main beam, which is a significant disadvantage, and thereby demands further optimization in order to overcome them [8].

Computer generated hologram for have been recently introduced in literature for multibeam synthesis [9-10]. However, the realization of dual-polarized TAs with desired radiation patterns is difficult, as the corresponding phase and magnitude requirements have to be realized independently for each polarization. In addition, the challenging task is to fulfill the requirements of orthogonal transmission phase modulation over the entire phase range of 360°, as well as the total transmission magnitude in both polarizations. In this regard, we combine the well-known Gerchberg-Saxton iterative method and a dual-polarized transmitarrays to synthetize a concentric dual-polarized flat-top radiation beam pattern. The proposed TA-GS

algorithm is an extension of GS algorithm for flat-top footprint pattern synthesis that accounts for the HTA effects such as the material losses at each iteration. The solution is carried-out without applying iterations or extra-computation cost to overcome the high sidelobe level. We evaluate the performance of phase correction in the HTA and investigate its cross-polarization discrimination (XPD) in order to validate its polarization diversity capability.

2 Proposed anisotropic HTA Unit-Cell

In our recent work [2], we have demonstrated a broadband anisotropic unit-cell based on a gridded Jerusalem-cross (GJC), which combines the inductive and capacitive behavior, and facilitates an independent phase control for two orthogonal linear polarizations. A different insertion loss is obtained for each TA phase shift. Unit-cells are printed on composite flexible dielectric substrate (Dupont Pyralux).

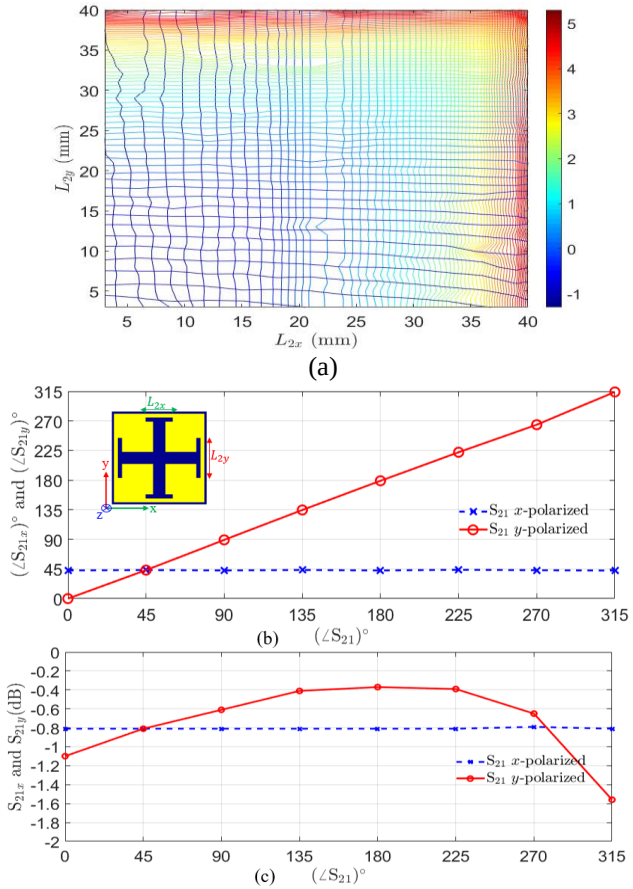

Figure 2: HFSS simulation: (a) 3D normalized susceptances b_x and b_y vs L_2, (b) simulated $\angle S_{21x}$ *and* $\angle S_{21y}$ vs desired $\angle S_{21}$ (c) $S_{21x}$and S_{21y}(dB) at desired $\angle S_{21}$.

The four stacked anisotropic layers achieve a full transmission phase coverage of 360°.

In fact, the polarizations must be orthogonal for two beams of the same coverage and frequency band. The fig.2a shows the contours of normalized susceptances b_x and b_y of one the four layers as a function of two varying arm lengths of the GJC, namely L_{2x} and L_{2y} (see [2] for details). The good orthogonality between the two sets of contours demonstrate that susceptances associated with x and y polarizations can be adjusted independently over a broad range of values. Although the susceptances, and therefore the phases, of the unit cell can be varied continuously, the TA can be efficiently designed by using a 3-bit phase quantization for each polarization, for a total of 64 possible phase states. Each cell was simulated with Ansys HFSS using a periodic boundary condition (PBC) (master-slave) and de-embedded Floquet ports. The frequency response of the broadband unit-cell were demonstrated in [2].

This Fig.2b illustrates two examples of achievable $\angle S_{21x}$ and $\angle S_{21y}$ simulated phases with respect to the desired ones. In this example, the phase of S_{21x} is fixed to 45 degrees and the 8 phase states of S_{21y} are achievable. Fig. 2c shows the corresponding insertion losses for these 8 states. The blue curve shows that S_{21x} remains constant while S_{21y} varies. It can be seen that the unit cell's insertion loss varies between 0.4 dB and 1.6 dB, depending on the applied phase.

3 Description of the TA-GS Algorithm

The HTA phase shift distribution is the component of interest allowing to synthetize the targeted far-field pattern. In order to present the proposed synthesis approach, the input incident wave has to be known.

For evaluating the performance of TA-GS algorithm and for the sake of simplicity, a "centered-circle flat-top" radiation pattern is demonstrated in this paper. In order to implement the discrete Fourier transform used for the TA-GS algorithm shown in Fig.3, we perform a zero-padding in order to improve pattern resolution in visible uv-plane then apply the FFT operation as required by the Nyquist sampling theorem. The design frequency is 20 GHz. At that frequency the size of the TA is 10.4λx10.4λ. Therefore, the numerical results presented here are for a TA of 52x52 cells.

A first validation study of the TA-GS algorithm has been performed with the TA illuminated with a theoretical Gaussian beam. The waist of this Gaussian beam has been varied to determine the required beamwidth of reference incident wave distribution illuminating the HTA. For a given polarization, either parallel (∥) or perpendicular (⊥), the equations below describe the iterations steps of the TA-GS procedure, as also illustrated in the flowchart diagram in Fig.3. Here, (x,y) refers to coordinates on unit cells in the TA plane and (u,v) to direction cosines in the far-field. Symbol "∘" in the following equations indicates the Hadamard product.

$$C(u,v) = I_0(u,v) \circ \exp(j\Psi_0(u,v)) \quad \text{(Eq0)}$$

$$\mathcal{F}^{-1}\{C(u,v)\} = E_B(x,y) \circ \exp(j\psi_B(x,y)) \quad \text{(Eq1)}$$

$$\Delta\varphi = \psi_i(x,y) - \psi_B(x,y) \quad \text{(Eq2)}$$

$$\psi_B^c(x,y) = \Delta\varphi(x,y) + \psi_i(x,y) \quad \text{(Eq3)}$$

$$c(x,y) = E(x,y) \circ \exp(j\psi_B^c(x,y)) \quad \text{(Eq4)}$$

$$E(x,y) = E_i(x,y) \circ T(x,y)$$

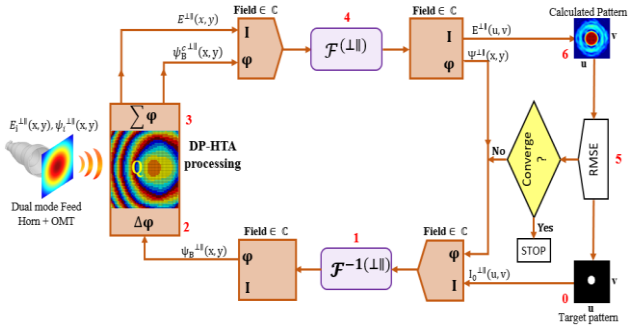

Figure 3: Workflow of the Dual-polarized TA-GS algorithm.

$$\hat{\mathrm{E}}(u,v) \circ \exp(j\Psi(u,v)) = \mathcal{F}\{E(x,y) \circ \exp(j\psi_B^c(x,y))\} \quad \text{(Eq5)}$$

$$RMSE = \left(\sum_{i,i} \left[\hat{\mathrm{E}}(u,v) - I_0(u,v) \right]^2 \right)^{0.5} \quad \text{(Eq6)}$$

Step 0: Specification of an initial input pattern, loaded as the amplitude distribution $I_0(u,v)$ of the desired far-field pattern. The phase distribution $\Psi_0(u,v)$ can be set to zero for the first iteration. See (Eq0).

Step 1: Back propagation from the far field to the HTA plane is performed with (Eq1).

Step 2: The HTA processing consists of three major operations in the spatial domain:

(a) $\Delta\varphi$ is the phase shift distribution applied by the HTA cells, that is, the difference between the phase of the incident wave on the HTA and the phase at the output of the HTA, as shown in equation (Eq2).

(b) The Q operator quantizes the $\Delta\varphi$ phase shifts into eight phase levels based on 3-bit quantization.

(c) A constant is added to the quantized HTA phase shift distribution in order to move the unit-cell with the best insertion loss at the center of the HTA. This ensures maximum power transfer. The related transmission coefficient magnitude distribution $T(x,y)$ obtained from the data collected from Fig.2c, is also determined.

Step 3: $\psi_B^c(x,y)$ calculated with (Eq3) provides the corrected backward propagator phase. The resulting field at the HTA output is obtained with (Eq4), where $E(x,y)$ is the amplitude distribution resulting from the incident wave $E_i(x,y)$ multiplied with the phase-dependent HTA transmission coefficient distribution $T(x,y)$.

Step 4: Next, the HTA output field distribution is transferred to the far-field (u,v) domain by using the fast Fourier transform (FFT according to (Eq5), where $\mathcal{F}\{.\}$ denotes the FFT operation; $\hat{\mathrm{E}}(u,v)$ and $\Psi(u,v)$ are respectively the amplitude and phase distributions.

Step 5: The difference between the estimated $\hat{\mathrm{E}}(u,v)$ and the target $I_0(u,v)$ patterns with a given threshold namely the normalized root-mean-square error (RMSE) which isused as a metric to determine the convergence.

Step 6: The TA-GS process is repeated iteratively until the goal (e.g., maximum iteration number or allowed RMSE is reached) is achieved.

4 Numerical results

In this section, we report numerical examples to validate the proposed method.

Here, the primary goal is to determine the optimal HTA phase distribution that can achieve a centered flat-top circular radiation pattern, with minimum sidelobes and ripples in the main beam. For demonstration, a 52x52 square array-antenna with an inter-element spacing of 0.2λ is chosen. The incident wavefront quality is an important factor, as it defines the accuracy of final radiation pattern. It depends on the distance of the HTA from the primary source, which is a dual mode horn antenna fed by an orthomode transducer (OMT). The field characteristics such as edge field intensity, edge illumination, half power beam width, (E, EI and HPBW) have been initially determined through a theoretical approach using Gaussian beam. Subsequently, the dual mode horn antenna is design in Ansys HFSS to provide the required incident wavefront. This is illustrated in Fig4.a and Fig4b for amplitude and phase distribution respectively.

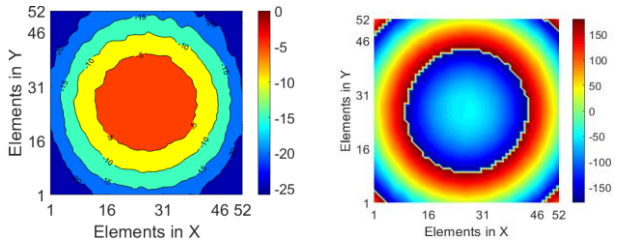

(a) (b)

Figure 4: Feed antenna field distribution in the HTA input plane : (a) amplitude (dB), (b) phase (°).

The HTA is placed at the focal distance of 170 mm from the dual-polarized feed antenna in order to obtain the desired edge field intensity. The amplitude distribution exhibits a half power beam width (HPBW) of 13°, while the required edge illumination EI = -11 dB, as magnitude of the taper allows acceptable spillover losses and sidelobes in the HTA far field.

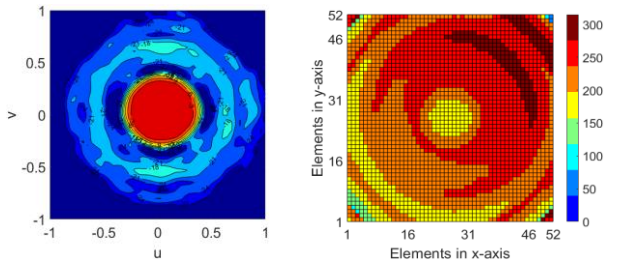

(a) (b)

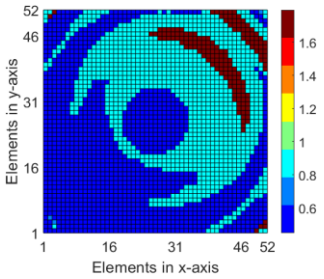

(c)

Figure 5: Results of the synthesis of a centered circular flat-top Far-field pattern: (a) amplitude of far-field pattern, (b) HTA phase-shift distribution, (c) HTA cells insertion loss distribution in dB.

The realized maximum sidelobe level is approximately -18 dB. The results show that the HTA-based optimum phase-shift and insertion loss distribution have a very smooth variation, leading to an efficient beam focusing.

5. Conclusion

In this study, we apply the TA-GS algorithm for dual-polarized beam shaping of concentric beams by a holographic-based dual-polarized transmitarray. First, by designing an anisotropic unit-cell, we were able to numerically demonstrate the generation of dual-polarized flat-top concentric beams with the same HTA aperture using a dual mode horn antenna. TA-GS algorithm features a rapid and robust approach. In this approach, sidelobe level and ripples are minimized inherently. The fabrication of a prototype to validate the proposed approach is underway.

6 References

[1] J. Huang and J. A. Encinar, Reflectarray Antennas, *NJ, Piscataway:Wiley-IEEE* Press, 2007.

[2] E. G. Plaza, G. Leon, S. Loredo and F. Las-Heras, "Dual polarized transmitarray lens", *2014 8th European Conference on Antennas and Propagation (EuCAP)*, pp. 2305-2308, 2014.

[3] L. N. A Bamogho, J.-J. Laurin and M A. Moharram, "Flexible Anisotropic Metasurface Transmitarray Unit Cell Design", *18th Int. Symp. Ant. Techn. App. Electrom. (ANTEM)*, Waterloo, Canada August 2018.

[4] H. Nematollahi, J. J. Laurin, J. E. Page, and J. A. Encinar, "Design of Broadband Transmitarray Unit Cells With Comparative Study of Different Numbers of Layers," *IEEE Trans. Antennas Propag.*, vol. 63, no. 4, pp. 1473–1481, Apr. 2015.

[5] E. G. Plaza, G. Leon, S. Loredo and F. Las-Heras, "Dual polarized transmitarray lens", *Proc. Eur. Conf. Antennas Propag. (EuCAP)*, pp. 2305-2308, The Hague, Netherlands, Apr. 2014.

[6] J. A. Encinar, L. Datashvili, J. A. Zornoza, M. Arrebola, M. Sierra-Castaer, J. L. Besada, et al., "Dual-polarization dual-coverage reflectarray for space applications", *IEEE Trans. Ant. Propagat.*, vol. 54, pp. 2827-2837, Oct. 2006.

[7] D. Boeringer and D. Werner, "Particle swarm optimization versus genetic algorithms for phased array synthesis", *IEEE Trans. Ant. Propagat.*, vol. 52, no. 3, pp. 771-779, Mar. 2004.

[8] W.P.M.N. Keizer, "Low sidelobe pattern synthesis using iterative Fourier techniques coded in MATLAB", *IEEE Antennas Propag. Mag*., vol. 51, no. 2, pp. 137-150, Apr. 2009.

[9] O. Yurduseven, D. R. Smith and T. Fromenteze, "Computational Millimeter-wave Spotlight Imaging using Holographic Metasurface Antennas", *2018 IEEE-APS URSI*, pp. 8-13, Boston, MA, USA, July 2018.

[10] O. Yurduseven and D. R. Smith, "Dual-polarization printed holographic multibeam metasurface antenna", *IEEE Antennas and Wireless Propagation Letters*, vol. 16, pp. 2738-2741, 2017.